Acta Geochim (2021) 40(4):473–483
https://doi.org/10.1007/s11631-021-00477-z

ORIGINAL ARTICLE

Variations of methane stable isotopic values from an Alpine peatland on the eastern Qinghai-Tibetan Plateau

Qian Guo[1,2,3] · Haijun Peng[1,3,4] · Bing Hong[1,3,4] · Hu Yao[1,2,3] · Yongxuan Zhu[1] · Hanwei Ding[1,2,3] · Ning An[1] · Yetang Hong[1]

Received: 12 March 2021 / Revised: 10 May 2021 / Accepted: 20 May 2021 / Published online: 3 June 2021
© Science Press and Institute of Geochemistry, CAS and Springer-Verlag GmbH Germany, part of Springer Nature 2021

Abstract Isotopic signature is a powerful tool to discriminate methane (CH_4) source types and constrain regional and global scale CH_4 budgets. Peatlands on the Qinghai-Tibetan Plateau are poorly understood about the isotopic signature of CH_4 due to the limited experimental conditions. In this study, three campaigns of diurnal air samples spacing 2–3 h were taken from an alpine peatland on the eastern Qinghai-Tibetan Plateau to investigate its source signal characteristics. Both CH_4 concentration and its stable carbon isotope ($\delta^{13}C$-CH_4) were measured to derive the carbon isotopic signature of the CH_4 source using the Keeling plot technique. Diurnal variation patterns in CH_4 concentration and $\delta^{13}C$-CH_4 were observed during summertime, with depleted $\delta^{13}C$-CH_4 signals and high CH_4 concentration appearing at nighttime. The $\delta^{13}C$-CH_4 signature during summer was calculated to be $-71\% \pm 1.3\%$, which falls within the range of other wetland studies and close to high-latitude peatlands. The boundary layer dynamic and CH_4 source were supposed to influence the measured CH_4 concentration and $\delta^{13}C$-CH_4. Further investigations of CH_4 isotopic signals into the non-growing season are still needed to constrain the $\delta^{13}C$-CH_4 signature and its environmental controls in this region.

Keywords Stable carbon isotope · Methane · Alpine peatland · Qinghai-Tibetan plateau · Diurnal variation

1 Introduction

Methane is an important greenhouse gas whose concentration has been rising again since 2007 after a general stabilization (Ueyama et al. 2020; Kirschke et al. 2013; Nisbet, Dlugokencky and Bousquet 2014; Nisbet et al. 2020; Jackson et al. 2020). CH_4 concentration does not include the source type information to determine definitively the causes of this recent rise, while the stable carbon isotope in CH_4 ($\delta^{13}C$-CH_4) could be a powerful tool to provide the source information. It has been suggested that global models should include specific isotopic signatures for wetlands from different regions due to their spatial and temporal variability (Sherwood et al. 2017).

Wetlands, especially peatlands, are distributed primarily in boreal and alpine regions (Chen et al. 2021). Many studies have reported the $\delta^{13}C$-CH_4 of wetlands in the high northern latitudes, but tropical and temperate wetlands are still understudied (Thottathil and Prairie 2021; Brownlow et al. 2017; Fisher et al. 2017). The Qinghai-Tibetan Plateau (QTP) is the largest and highest plateau in the world, with an average elevation of over 4,000 m (Zhang et al. 2020; Wang et al. 2015). This plateau developed large amounts of peatland owing to its unique alpine environment, which accounts for 49% (5,086 km^2) of the total peatland areas and 68% (1.49 Pg C) of total peatland C

✉ Haijun Peng
penghaijun@mail.gyig.ac.cn

✉ Bing Hong
hongbing@vip.skleg.cn

1 State Key Laboratory of Environmental Geochemistry, Institute of Geochemistry, Chinese Academy of Sciences, Guiyang 550081, China

2 University of Chinese Academy of Sciences, Beijing 100049, China

3 Bayinbuluk Alpine Wetland Carbon Flux Research Station, Chinese Flux Observation and Research Network, Beijing, China

4 CAS Center for Excellence in Quaternary Science and Global Change, Xi'an 710061, China

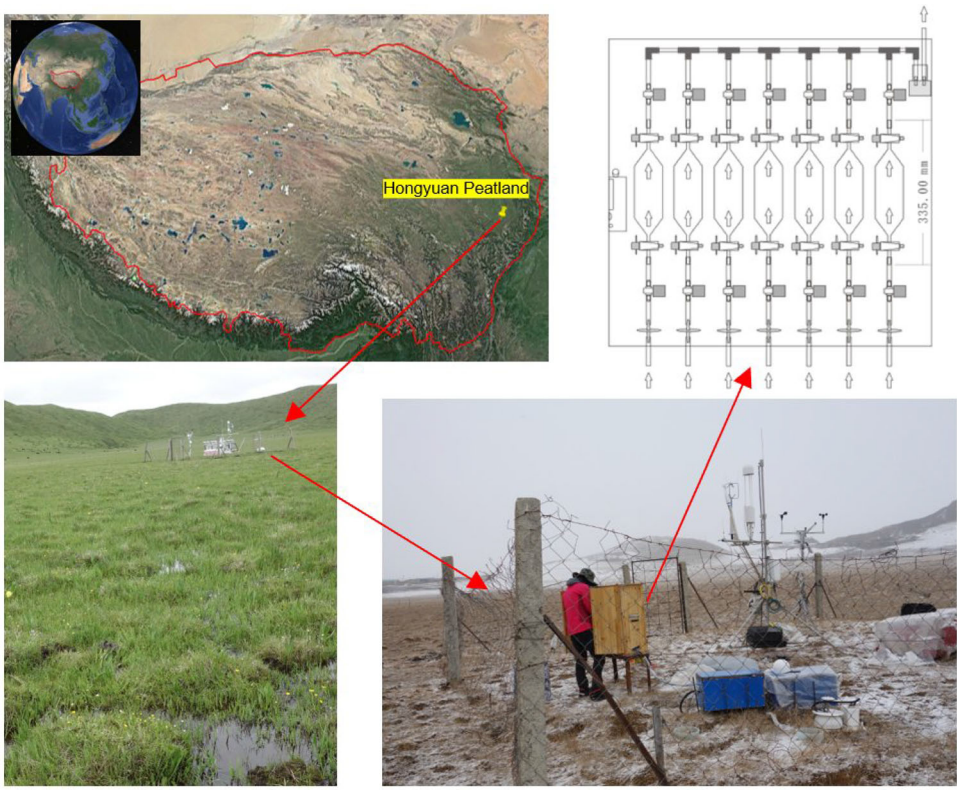

Fig. 1 Maps showing the location of QTP (red solid line) and Hongyuan peatland (yellow pin), summer site view of the eddy covariance tower, and the weather station in Hongyuan peatland, automatic air sampler used in this study and its design drawing

storage in China (Yang et al. 2017). The Zoigê peatland, known as the largest alpine peatland in the world, is located on the eastern edge of the QTP (Xiang et al. 2009; Yao et al. 2011). Besides the high elevation, these peatlands are influenced both by the Indian Summer Monsoon and East Asia Summer Monsoon, making them particularly susceptible to global climate changes (Yang et al. 2010; Zhang et al. 2021). Most previous studies on CH_4 emissions of the Zoigê peatland were focused on their inter-annual variations and regional budget estimation (Hirota et al. 2004; Chen et al. 2009, 2013, 2021; Song et al. 2015; Wei et al. 2015; Peng et al. 2019). Chen et al. (2021) reported the CH_4 fluxes characteristics in different periods (especially in the freeze–thaw period) on the Zoigê peatland. Peng et al. (2019) found the diurnal and seasonal variations of CH_4 fluxes and discussed the key environmental factors that affected the CH_4 emissions on a Zoigê peatland. Measurement of changing CH_4 concentration and $\delta^{13}C\text{-}CH_4$ value could determine sources of CH_4 on a regional scale (Fisher et al. 2006). Due to the limited experimental conditions, few studies were conducted about the $\delta^{13}C\text{-}CH_4$ characteristics of the Zoigê peatland.

Kato et al. (2013) firstly used $\delta^{13}C\text{-}CH_4$ value to help understand the soil CH_4 consumption and production through the chamber samples in the alpine ecosystems on the QTP. Though chamber measurements can help explain the mechanisms (Zhang et al. 2011; Chanton et al. 2008, Rao, Bhattacharya and Jani 2008), but cannot provide a consistent isotopic signature to represent larger-scale processes. Recent studies showed that samples from ambient air can contain a well-mixed air above the soil surface and provide a more coherent regional scale $\delta^{13}C\text{-}CH_4$ signature (Fisher et al. 2017; Banda et al. 2016; Rockmann et al. 2016; Morimoto et al. 2017). To the present, little is known about the $\delta^{13}C\text{-}CH_4$ signature in ambient air on the Zoigê peatland which could use in large-scale studies.

To obtain the isotopic signature, we deployed an automatic gas sampler near an eddy covariance (EC) CH_4 flux tower in a peatland on the QTP and used the Keeling plot technique (Keeling 1958) to identify the isotopic inputs of CH_4 in this region. The research objectives, therefore, are to (1) reveal the temporal variation of the $\delta^{13}C\text{-}CH_4$ from alpine peatlands on the QTP, (2) compare the $\delta^{13}C\text{-}CH_4$ signatures from various peatlands at different latitudes, and (3) lay a foundation for applying this technique to the studies of CH_4 from other peatlands in China.

2 Materials and methods

2.1 Study site

The study site, Hongyuan Peatland (32°46′N, 102°30′E), located around 3 km southwest of the Hongyuan County at

an altitude of around 3510 m above sea level, is part of the Zoigê peatlands on the eastern QTP (Fig. 1). The dominant plants in this peatland are *Carex mulieensis* and *Kobresia tibetica* (Peng et al. 2019). The mean annual temperature and precipitation are 1.8 °C and 746 mm, respectively (http://data.cma.cn/). The highest monthly mean air temperature is typically observed in July (11.2 °C on average), whereas the lowest is in January with a 30-year mean of −9.4 °C. More than 75% of annual precipitation usually occurs during the growing season from May to September each year.

2.2 Sampling and analytical procedure

The air samples were collected using an automatic sampler at a height of 50 cm above the soil surface. The sampler was composed of a GSM remote controller, a battery-operated pump (flow rate 4–5 L/min), 14 replaceable 300 mL flasks, and the necessary valves (Fig. 1). The sampler collects air samples via opening and closing the pump and the valves at the end of the flasks which got command of the GSM controller. Samples were collected in 3 h intervals for 24 h and then shipped to the laboratory for further analysis.

Air samples were first analysed for CH_4 concentrations using a Gas Chromatograph (GC) with a Flame Ionization Detector system (HP 6890, Agilent Technologies Co. Ltd, USA). Then the rest samples were used to measure δ^{13}C-CH_4 by the Trace Gas pre-concentrator (TG PreCon) and IsoPrime mass spectrometer (GV Instruments, UK). This isotope measurement system had repeatability of better than 0.5% for δ^{13}C-CH_4. Air samples firstly entered the TG PreCon system through the dual—ended sample flask. A helium flow (99.999% purity) then transported the air sample through several chemical traps and a liquid nitrogen cryotrap held at −196 °C to remove water, CO, and CO_2. The rest sample flowed into the combustion furnace where CH_4 was oxidized to CO_2. The resultant CO_2 was trapped and cryofocused in the liquid nitrogen and then passed through the GC column to filter out other residual gas substances. Finally, the flow went to the IsoPrime mass spectrometer for isotopic measurement. The isotopic analysis used CO_2 as the working reference which was calibrated against the MAT 252 mass spectrometer (Finnigan MAT, Germany). Additionally, to make sure there was no significant drift when CH_4 was oxidized to CO_2, several referenced air samples containing the similar CH_4 concentration were measured before and during the real samples. δ^{13}C-CH_4 represents the $^{13}C/^{12}C$ ratio in a sample relative to that of the standard (Vienna Pee Dee Belemnite) and are calculated as follows:

$$\delta^{13}\mathrm{C}(\%) = \left(\frac{\mathrm{R_{sample}}}{\mathrm{R_{std}}} - 1\right) \times 1000 \quad (1)$$

where R_{sample} and R_{std} are the $^{13}C/^{12}C$ ratio of the sample and the standard, respectively.

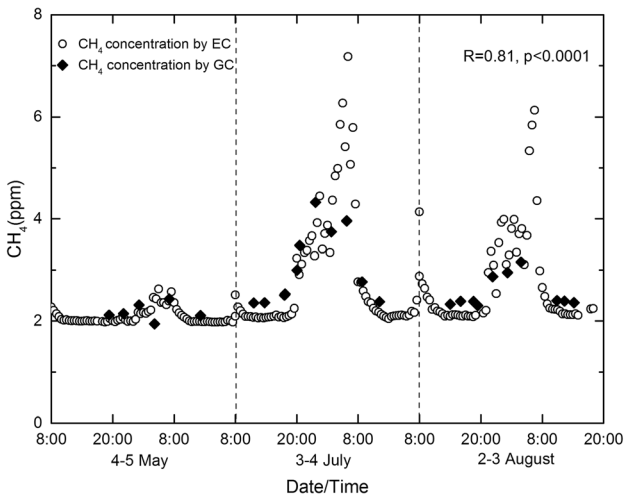

Fig. 2 CH_4 concentrations measured by the LI-7700 analyser and the GC system

2.3 Calculating source signature of δ^{13}C-CH_4

The Keeling plot technique, first proposed by Keeling (1958), is used for the δ^{13}C-CH_4 signature calculation. It is based on the following mass conservation:

$$c_a = c_b + c_s \quad (2)$$

$$c_a\delta^{13}C_a = c_b\delta^{13}C_b + c_s\delta^{13}C_s \quad (3)$$

where c_a, c_b, c_s are the atmospheric CH_4 concentration, the background CH_4 concentration, and source CH_4 concentration, respectively. δ^{13}C represents the carbon isotope ratio of each CH_4. By combining these two equations, a linear regression equation could be used to derive the intercept as the source or mixture source signature by plotting of δ^{13}C versus 1/concentration as follow:

$$\delta^{13}C_a = \delta^{13}C_s + \left[c_b\left(\delta^{13}C_a - \delta^{13}C_s\right)\right]/c_a \quad (4)$$

When using this method, it is assumed that there are no variations of δ^{13}C in both background and source during a short observation period, for example, a 24-h period in this study. Additionally, we used the geometric mean regression suggested by Pataki et al. (2003).

2.4 CH_4 fluxes and ancillary measurements

Methane fluxes were measured by an eddy covariance system sitting 2.5 m above the ground. This system consists of an open-path infrared CH_4 analyser (LI-7700, LI-COR Inc., USA), an open-path infrared CO_2/H_2O analyser

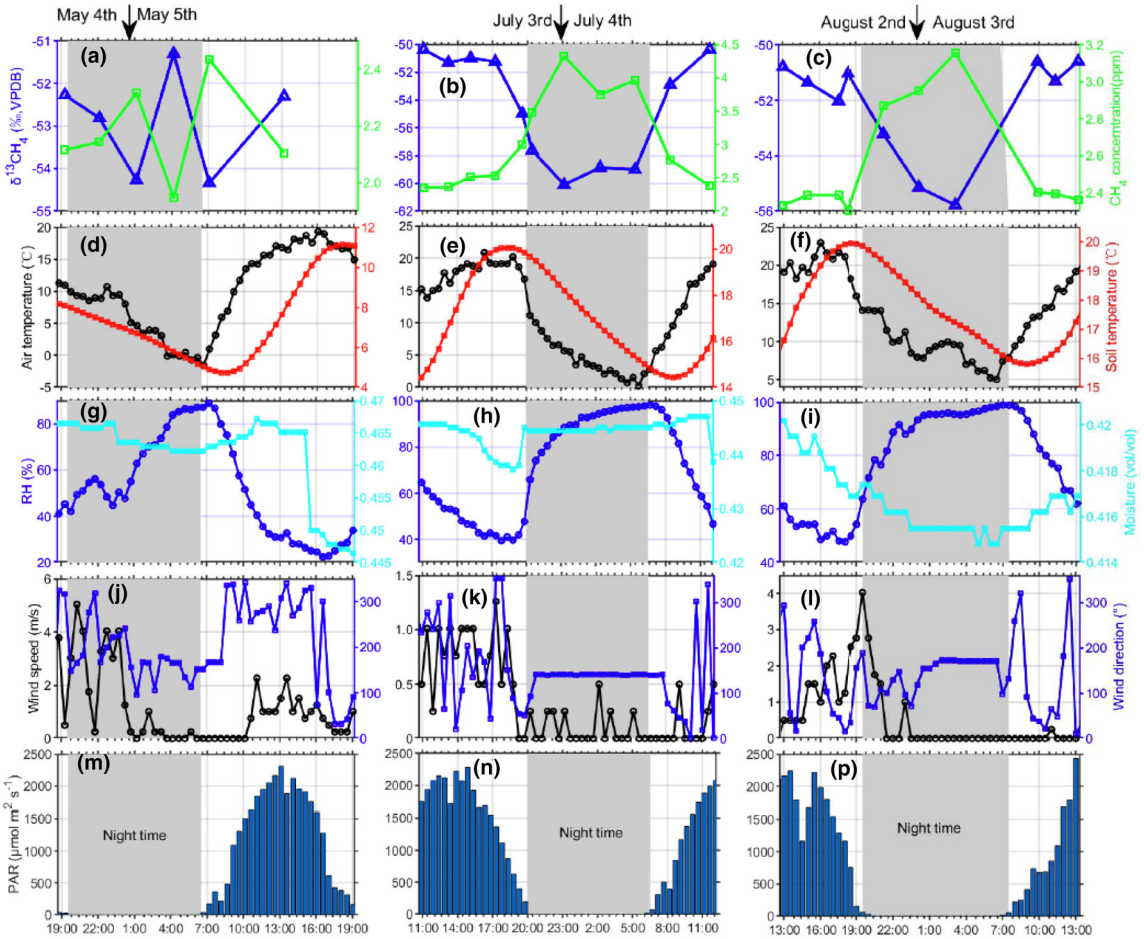

Fig. 3 Diurnal variations in δ^{13}C-CH_4, CH_4 concentration, and environmental factors during the three campaigns (Beijing time, GMT + 8). **a**, **b** and **c** are δ^{13}C-CH_4 and CH_4 concentration; **d**, **e**, and **f** are air temperature and soil temperature at the depth of 10 cm; **g**, **h**, and **i** are relative humidity (RH) and moisture; **j**, **k**, and **l** are wind speed and wind direction; **m**, **n**, and **p** were photosynthetically active radiation (PAR)

(LI-7500A, LI-COR Inc., USA), and an ultrasonic anemometer (WindMaster Pro, Gill Instruments Limited, UK). The half-hourly average flux was calculated by the EddyPro 5.01software (LI-COR Inc., USA) (details were provided in Peng et al. (2019)). Other ancillary environmental measurements, including global radiation, air temperature, relative humidity (RH), precipitation, soil temperature at three depths (10, 25, and 40 cm below the ground), and soil water content at the depth of 10 cm, were measured and recorded by a HOBO U30 weather station installed near the EC tower (Fig. 1) (Peng et al. 2015).

3 Results

3.1 Diurnal variations of CH_4 and environmental conditions

Three campaigns were deployed during the following three periods: 4–5 May, 3–4 July, and 2–3 August of 2016. To test the reliability of air samples from flasks during the sampling and transportation process, we first compared the CH_4 concentrations measured by the EC system and GC system. From Fig. 2, there is a good match of CH_4 concentrations detected by these two methods ($R = 0.81$, $p < 0.0001$) and the air samples could well capture the variations in CH_4 concentrations during the three campaigns, especially during 3–4 July and 2–3 August. Therefore, we can ignore the deviation of the samples that may occur during the sampling and transportation process.

The CH_4 concentrations and δ^{13}C values are shown in Fig. 3a, b, c. Clear diurnal patterns in CH_4 concentrations were observed during 3–4 July and 2–3 August, whereas no similar variation of CH_4 concentrations was seen in 4–5 May. The lower CH_4 concentrations were measured in the daytime and the higher CH_4 concentration in the nighttime during 3–4 July and 2–3 August. The CH_4 concentration ranged from 1.95–4.32 ppm during the three campaigns. The lowest concentrations were observed during 4–5 May,

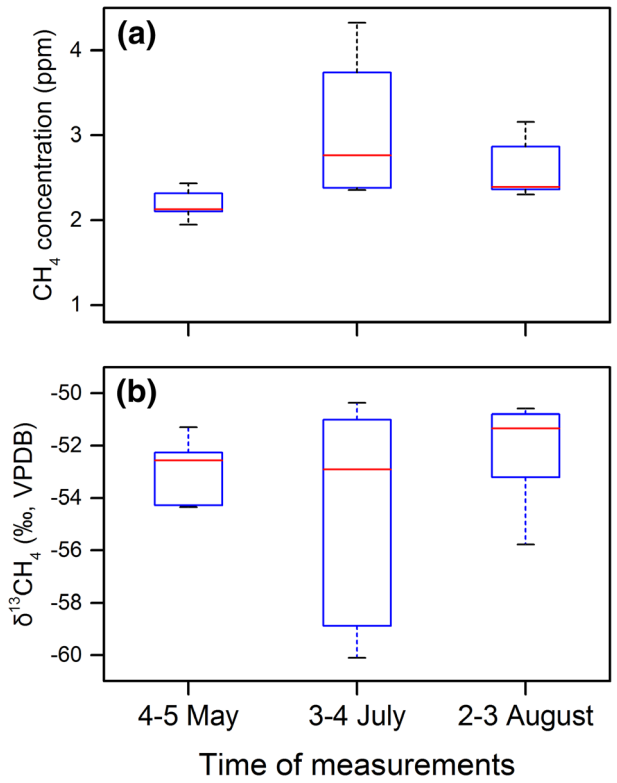

Fig. 4 Box and whisker showing **a** CH_4 concentrations, and **b** δ^{13}C-CH_4 of air samples during the three campaigns. Red lines represent median values

ranging from 1.95–2.43 ppm, while the higher values were observed in 3–4 July and 2–3 August, ranging from 2.36–4.32 ppm and from 2.3–3.16 ppm, respectively. From Fig. 4a, the largest daily amplitude (1.97 ppm) was observed during 3–4 July, and smaller daily amplitudes were seen during 4–5 May (0.49 ppm) and 2–3 August (0.85 ppm). The average CH_4 concentration were 2.18, 3.04, and 2.55 ppm in May, July, and August, respectively.

The δ^{13}C-CH_4 was tightly concomitant with the variations in CH_4 concentrations (Fig. 3a, b, c). The higher δ^{13}C-CH_4 was measured in the daytime and the lower δ^{13}C-CH_4 in the nighttime. The δ^{13}C-CH_4 ranged from −54.34% to −51.3%, −60.1% to −50.37% and −55.78% to −50.59% in 4–5 May, 3–4 July, and 2–3 August, respectively. From Fig. 4b, the largest daily amplitude was seen during 3–4 July, with the value of 9.73%, and smaller daily amplitudes were seen during 4–5 May and 2–3 August, with the values of 3.04% and 5.19%. The average δ^{13}C-CH_4 were −52.88%, −54.35% and −52.18% in 4–5 May, 3–4 July, and 2–3 August, respectively.

Both the air temperature and soil temperature at the depth of 10 cm showed similar diurnal changes with an increase in the daytime and a decrease in the nighttime (Fig. 3d, e, f). The average air temperature was 9.8, 11, 13.3 °C in 4–5 May, 3–4 July, and 2–3 August, respectively, ranging from −1.6 to 19.3 °C, 0–20.9 °C, 5–23 °C in 4–5 May, 3–4 July and 2–3 August, respectively. Average soil temperature was 7.3, 17, 17.7 °C, varying from 4.7–11.1 °C, 14.4–20 °C, 15.8–20 °C in May, July, and August, respectively.

The daily-average relative humidity (RH) was relatively low in 4–5 May (53%) and increased to 72% and 78% in 3–4 July and 2–3 August, respectively (Fig. 3g, h, i). Accordingly, the RH showed similar trends in 3–4 July and 2–3 August with a rapid increase and then stay at high values in the nighttime and a relatively slow decrease in the daytime. While the trend in 4–5 May was a relatively slow increase to reach a peak in the daytime and gradually decreased in the nighttime. The diurnal changes in moisture were, on average, 0.462, 0.444, and 0.417 vol/vol, respectively, varying from 0.446–0.467 during 4–5 May, from 0.437–0.447 during 3–4 July, and from 0.415–0.42 during 2–3 August, which appeared to decrease from May to August (Fig. 3g, h, i).

The diurnal variations of wind speed were quite different among the three campaigns (Fig. 3j, k, l). For the campaign on 4–5 May, the wind speed was variable quickly from higher values to lower values (< 2 m/s) during the first half of the night and then dropped to the lowest wind speed until the end of the next daytime, while low wind speed occurred (< 2 m/s) during all night of 3–4 July and 2– August (Fig. 3j, k, l). Wind direction was almost constant in the nighttime of 3–4 July and 2–3 August while was highly variable in the nighttime of 4–5 May. Photosynthetically active radiation (PAR) showed a clear diurnal pattern with a progressive increase in the daytime, which was similar to the change of the air temperature (Fig. 3m, n, p).

3.2 Long-time variations of CH_4 and environmental conditions

CH_4 flux and environmental variables from May to August of 2016 were all shown in Fig. 5. CH_4 flux showed a distinct increase from May to August (Fig. 5a), with the peak occurred from July to August. δ^{13}C-CH_4 values were more depleted in July than those in May and August. Daily mean air temperature became higher in July and August compared with that in May. Soil temperature from different depths also showed an increase in July and August than in May. PAR showed a constant oscillation during the observation time. More precipitation occurred from July to August than that in May. Soil moisture at the depth of 10 cm was influenced by both soil temperature and precipitation (Peng et al. 2019).

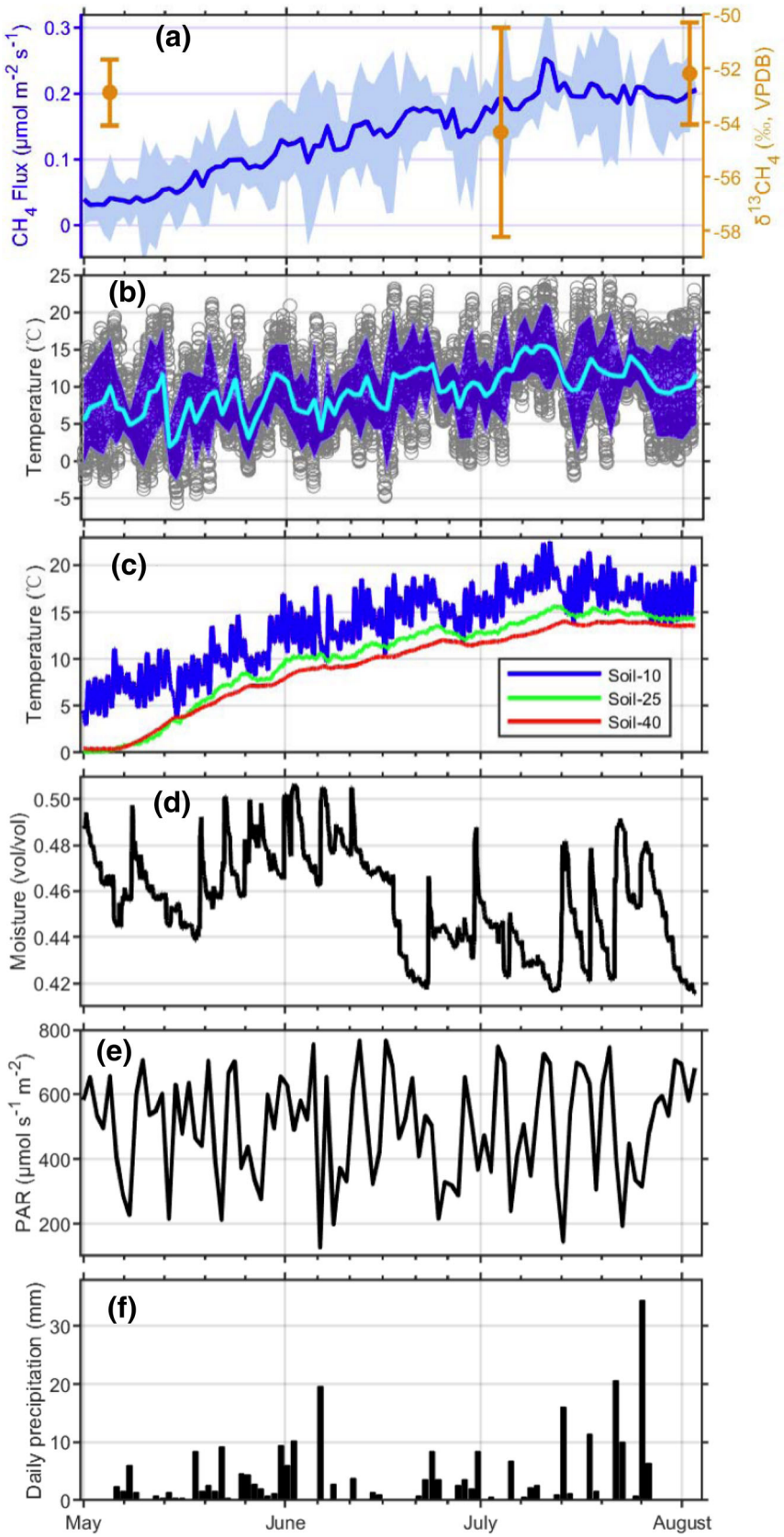

Fig. 5 **a** CH_4 flux (the blue line stands for daily mean fluxes and the shaded area denotes the standard deviation for each half-hour interval) and measured $\delta^{13}C\text{-}CH_4$ of the three campaigns, **b** air temperature (the grey circles are the half-hourly observation, the light blue line shows the daily mean air temperature and the shaded area represents the standard deviation for each half-hour interval, c soil temperature at the depth of 10, 25, and 40 cm, respectively, **d** soil moisture at the depth of 10 cm, **e** PAR and f daily precipitation from May to August of 2016

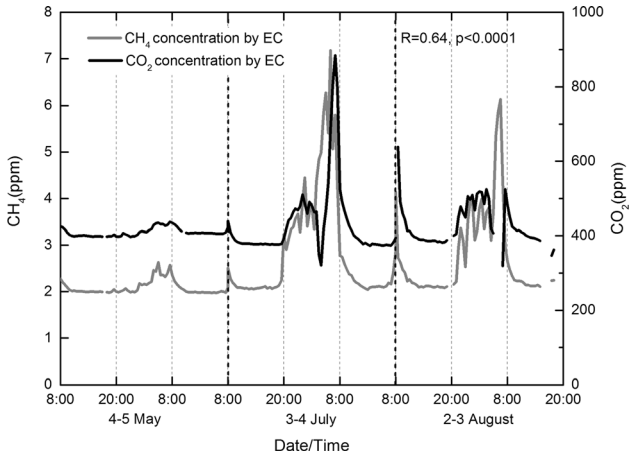

Fig. 6 CH_4 concentrations and CO_2 concentrations measured by the EC system

4 Discussion

4.1 Diurnal patterns of CH_4 concentration and δ^{13}C-CH_4

The campaigns on 3–4 July and 2–3 August had obvious diurnal variations and large variation ranges in both CH_4 concentration and δ^{13}C-CH_4, while the campaign in 4–5 May showed unclear diurnal change and a small variation range of CH_4 concentration and δ^{13}C-CH_4 (Fig. 3) (Fig. 4). In addition, the CH_4 concentrations and CO_2 concentrations measured by the EC system on this study area had similar diurnal cycles (Fig. 6). These results may represent that the variations of methane were mainly influenced by the boundary layer dynamic on the daily scale and influenced by the emitting source on the long-time scale (Lowry et al. 2001).

For the daily scale, the variation of boundary layer height cannot directly affect the CH4 concentrations and δ^{13}C-CH_4 from the source but can affect the observation of methane build-up in the ambient air. In general, an overnight build-up of CH4 concentration occurs during stable nocturnal boundary layer after sunset and disperses into the expanding boundary layer when temperature inversion broke during sunrise. Lowry et al., (2001) pointed out that the large variation of air temperature under the conditions of low wind speed could lead to the development of strong low-level inversion. Therefore, the beneficial meteorological condition could be helpful to observe an obvious build-up of methane. Our results showed that the three campaigns all had a large variation in air temperature, but the low wind speed of nighttime only occurred during 3–4 July and 2–3 August (Table 1), which could significantly slow down the mixing of CH4 concentration. During the campaign of 4–5 May, we did not observe a strong nighttime build-up of methane, possibly because of the lack of development of a stable nocturnal boundary layer (Sriskantharajah et al. 2012). In addition, the small amount of observation data during 4–5 May may also not capture the obvious build-up of methane. For the long-time scale, the variation of the methane may affect by the source and will discuss in the next section.

4.2 Identification of δ^{13}C-CH_4 signatures and their variations

Based on the Keeling plot technique, δ^{13}C-CH_4 signatures were derived from the three campaigns (Fig. 7). The δ^{13}C-CH_4 signature was $-68.30\% \pm 1.6\%$, $-2.39\% \pm 0.8\%$ and $69.49\% \pm 1.8\%$ for 4–5 May, 3–4 July, and 2–3 August, respectively. The δ^{13}C-CH_4 signature of 3–4 July showed the most depleted value compared with the other two campaigns. To compare with other wetland studies, we put all the data from the three campaigns together and found that the data from 3–4 July and 2–3 August had a better correlation ($R = 0.98$, $p < 0.0001$) when excluded the data during 4–5 May, therefore we derived a summer δ^{13}C-CH_4 signature of $71\% \pm 1.3\%$ for this study area (Fig. 7d).

During 4–5 May, the measured CH_4 concentration was significantly lower than those in summer and the δ^{13}C-CH_4 signature showed an approximate 3% increase compared with the summer signature, which may imply a potential variation of methane from source on a long-time scale. It has been noted that both the CH_4 production process and its transport path can affect its δ^{13}C-CH_4 composition (Conrad 2005; Popp et al. 1999). Sriskantharajah et al. (2012) observed that δ^{13}C-CH_4 emitted in the spring thaw was more enriched in δ^{13}C than that in summer from a subarctic

Table 1 CH_4 concentration, δ^{13}C-CH_4, air temperature, and wind speed during the observation period

Sampling time	Amplitudes of CH_4 concentration (ppm)	Amplitudes of δ^{13}C-CH_4 (‰)	Air temperature (°C)			Mean wind speed (m/s)	
			Max	Min	Mean	Daytime	Nighttime
4–5 May	0.49	3.04	19.3	1.6	9.8	1	1.2
3–4 July	1.97	9.73	20.9	0.2	11.0	0.5	0.2
2–3 August	0.85	5.19	23.0	5.0	13.3	1.0	0.2

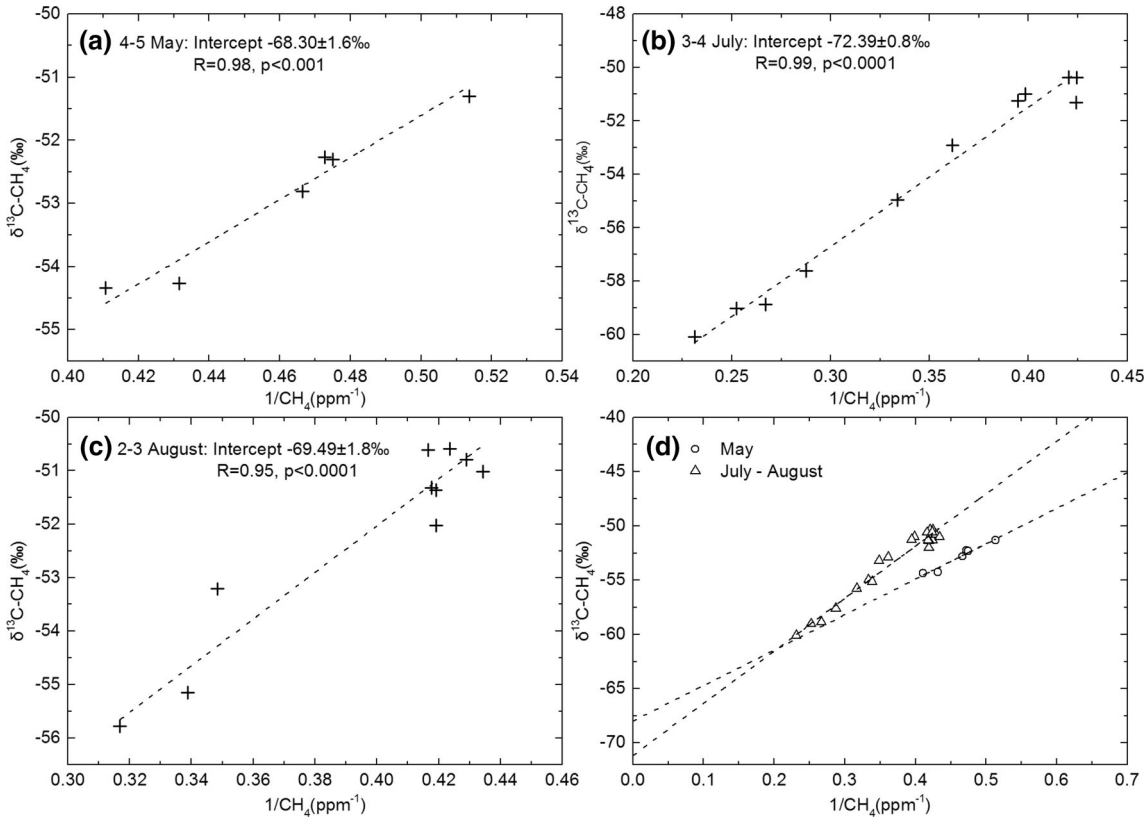

Fig. 7 Keeling plots for each campaign and their comparison. **a**-**c** Three cases during 4–5 May, 3–4 July, and 2–3 August, **d** Results during May and results combined with data of July and August. The intercepts of the y-axis represent the carbon isotopic signature of methane inputs in this region

wetland, which is similar to this study. Rao et al. (2008) also found a significant seasonal change of δ^{13}C-CH_4 over the paddy fields, with enriched δ^{13}C-CH_4 at the beginning and the end of the growing season, and depleted δ^{13}C-CH_4 before harvesting. In this study, the plants haven't started to grow in 4–5 May, and CH_4 flux was quite low and other environmental factors were distinctly different from those during summer (Fig. 5), which may result in the lower emitted CH_4 concentration. During July to August, CH_4 flux almost reached the peak values and biomass growth provided more substrates input in the form of root exudates to the anaerobic microbial community compared with the original substrates in May (Bergman, Klarqvist and Nilsson 2000), which lead to an increase of CH_4 concentration and more depleted ^{13}C in the emitted CH_4. In addition, part of the produced CH_4 can be transported into the air by abundant aerenchyma, this could also cause significant fractionation and thus result in the depletion in δ^{13}C-CH_4 in summer (Schütz and Rennenberg 1991; Chanton 2005; Happell et al. 1993). Since the data of this study were too small to further test the seasonal variation of δ^{13}C-CH_4 in this region, more investigation should be done in the future study, especially in the non-growing season.

4.3 Global wetland δ^{13}C-CH_4 signatures comparison

To our best, we compiled the existing published data of the δ^{13}C-CH_4 from wetlands at different latitudes, the results show that δ^{13}C-CH_4 signatures at lower latitude are around −60%, e.g., Amazon floodplain (53%), Florida Everglades (−55%), Thailand Swamp (66.1%) and Minnesota peatland (−67%), whereas at high latitude, δ^{13}C-CH_4 signatures are around −70% (Table 2). Ganesan et al., (2018) also found a large difference of 10% between boreal signature (67.8%) and tropical signature (56.7%) from wetlands using the inverse model. It seemed that δ^{13}C-CH_4 signatures from high latitude are more depleted in ^{13}C than those from lower latitude.

Though the location of Hongyuan Peatland belongs to the mid-latitude area, the summer δ^{13}C-CH_4 signature of −71% is much closer to those of the high-latitude studies. This could be explained by the low air temperature and alpine environment, which are similar to the boreal wetlands at the high latitude rather than the warm wetlands at the low latitude. For boreal wetlands at the high-altitude, the depleted δ^{13}C-CH_4 could be attributed to the following reasons: (1) the ^{13}C of the organic material in the sediments

Table 2 Comparison with $\delta^{13}C\text{-}CH_4$ from other published studies

Study Country	Environment	Sampling method	Sampling period	Mean $\delta^{13}C\text{-}CH_4$ (‰)	References
USA	Minnesota peat bogs	Chamber, bubbles, water, ambient air samples	May–June 1986	−66	Quay et al. (1988)
	Alaska tundra		August 1987	−64	
	Amazon floodplain		July–August 1985 and May 1987	−53	
USA	Minnesota peatland	Ambient air samples	June	−67	Stevens and Engelkemeir (1988)
	Florida Everglades		October–November	−55	
Russia	Russia wetlands	Ambient air samples	August	−62.4	Bergamaschi et al. (1998)
Thailand	Thailand Swamp	Bubbles	Summers and winters	−66.1	Nakagawa et al. (2002)
Russia	North Siberian lakes	Bubbles	July 2001, May 2003&June 2004	−70	Walter et al. (2008)
	Western Siberian wetland	Aircraft	July–September	−70	Umezawa et al. (2012)
Russia	Russia wetlands	Aircraft	July	−70	France et al. (2016)
Europe	Boreal wetlands (forest and peat bogs)	Chamber, ambient air samples, aircraft	July–October	−71	Fisher et al. (2017)
Tropical area	wetlands	Ambient air samples	2014–2016	−61.5 ~ −53	Brownlow et al. (2017)
High-latitude area	wetlands	inverse model	–	−67.8	Ganesan et al. (2018)
Tropical area	wetlands	inverse model	–	−56.7	Ganesan et al. (2018)
Canada	Boreal lakes	Bubbles and diffusion	May–November	55.9	Thottathil and Prairie (2021)
China	Zoigê peatland	Ambient air samples	July–August	−71	This study

is more depleted at high latitudes due to a temperature dependence of kinetic and equilibrium isotope effects that occur during photosynthesis (Stevens and Engelkemeir 1988); (2) high-altitude wetlands have thinner oxic layers than those at low latitude, which could lead to less CH_4 oxidation (Brownlow et al. 2017); (3) the differences in methanogenic communities could also lead to the depletion of ^{13}C (Fisher et al. 2017).

5 Conclusions

In this study, carbon isotopic signatures of CH_4 in a Zoigê alpine peatland are determined via collecting air samples upon the soil surface from May to August of 2016. CH_4 concentration measured by the LI-7700 open-path analyser is in line with that measured by the GC system. Clear diurnal variation patterns of CH_4 concentration and $\delta^{13}C\text{-}CH_4$ were observed throughout the study period, which was mainly influenced by boundary layer dynamics. Long-time variations in CH_4 concentration and $\delta^{13}C\text{-}CH_4$ may be dominated by the CH_4 source. Our results provide a non-intrusive method to employ the source signature of methane and give a summer $\delta^{13}C\text{-}CH_4$ signature of −71% of the QTP peatland which is close to the signature at the high-latitude area. However, more investigations into long-time, especially non-growing season, of $\delta^{13}C\text{-}CH_4$ variation patterns in this understudied region are still required to decipher the regional CH_4 source signature and their environmental controllers.

Author contributions H.P. and B.H designed the study. Q.G., H.Y, and H.D conducted field works. Q.G., Y.Z., and N.A. conducted laboratory analysis. Q.G. and H.P. conducted data analysis and wrote the first draft of the manuscript. All co-authors were involved in the discussion and revising of the manuscript.

Funding This research was financially supported by the Strategic Priority Research Program of Chinese Academy of Sciences (Grant No. XDB40010000), the National Natural Science Foundation of China (Grant Nos. 41907288, 41673119, and 41773140), and the Science and Technology Foundation of Guizhou Province (Grant Nos.

[2019]1317 and [2020]1Y193). H. P. was supported by the "Light of West China" Program and the CAS Scholarship.

Declaration

Conflict of interest The authors declare that they have no conflict of interest.

References

Banda N, Krol M, van Weele M, van Noije T, Le Sager P, Rockmann T (2016) Can we explain the observed methane variability after the Mount Pinatubo eruption? Atmos Chem Phys 16:195–214

Bergamaschi P, Brenninkmeijer CAM, Hahn M, Rockmann T, Scharffe DH, Crutzen PJ, Elansky NF, Belikov IB, Trivett NBA, Worthy DEJ (1998) Isotope analysis based source identification for atmospheric CH_4 and CO sampled across Russia using the Trans-Siberian railroad. J Gerontol Ser A Biol Med Sci 103:8227–8235

Bergman I, Klarqvist M, Nilsson M (2000) Seasonal variation in rates of methane production from peat of various botanical origins: effects of temperature and substrate quality. FEMS Microbiol Ecol 33:181–189

Brownlow R, Lowry D, Fisher RE, France JL, Nisbet EG (2017) Isotopic ratios of tropical methane emissions by atmospheric measurement. Global Biogeochem Cycl. https://doi.org/10.1002/2017GB005689

Chanton JP (2005) The effect of gas transport on the isotope signature of methane in wetlands. Org Geochem 36:753–768

Chanton JP, Glaser PH, Chasar LS, Burdige DJ, Hines ME, Siegel DI, Tremblay LB, Cooper WT (2008) Radiocarbon evidence for the importance of surface vegetation on fermentation and methanogenesis in contrasting types of boreal peatlands. Global Biogeochem Cycl. https://doi.org/10.1016/j.orggeochem.2004.10.007

Chen H, Wu N, Yao S, Gao Y, Zhu D, Wang Y, Xiong W, Yuan X (2009) High methane emissions from a littoral zone on the Qinghai-Tibetan Plateau. Atmos Environ 43:4995–5000

Chen H, Wu N, Wang Y, Zhu D, a Zhu Yang Gao Fang Wang Peng QGYXXC (2013) Inter-annual variations of methane emission from an open fen on the Qinghai-Tibetan Plateau: a three-year study. PLoS ONE 8:e53878

Chen H, Liu X, Xue D, Zhu D, Zhan W, Li W, Wu N, Yang G (2021) Methane emissions during different freezing-thawing periods from a fen on the Qinghai-Tibetan Plateau: Four years of measurements. Agric for Meteorol 297:108279

Conrad R (2005) Quantification of methanogenic pathways using stable carbon isotopic signatures: a review and a proposal. Org Geochem 36:739–752

Fisher R, Lowry D, Wilkin O, Sriskantharajah S, Nisbet EG (2006) High-precision, automated stable isotope analysis of atmospheric methane and carbon dioxide using continuous-flow isotope-ratio mass spectrometry. Rapid Commun Mass Spectrom 20:200–208

Fisher RE, France JL, Lowry D, Lanoiselle M, Brownlow R, Pyle JA, Cain M, Warwick N, Skiba UM, Drewer J, Dinsmore KJ, Leeson SR, Bauguitte SJB, Wellpott A, O'Shea SJ, Allen G, Gallagher MW, Pitt J, Percival CJ, Bower K, George C, Hayman GD, Aalto T, Lohila A, Aurela M, Laurila T, Crill PM, McCalley CK, Nisbet EG (2017) Measurement of the ^{13}C isotopic signature of methane emissions from northern European wetlands. Global Biogeochem Cycl 31:605–623

France JL, Cain M, Fisher RE, Lowry D, Allen G, O'Shea SJ, Illingworth S, Pyle J, Warwick N, Jones BT, Gallagher MW, Bower K, Le Breton M, Percival C, Muller J, Welpott A, Bauguitte S, George C, Hayman GD, Manning AJ, Myhre CL, Lanoiselle M, Nisbet EG (2016) Measurements of δ13C in CH4 and using particle dispersion modeling to characterize sources of Arctic methane within an air mass. J Gerontol Ser A Biol Med Sci 121:14257–14270

Ganesan AL, Stell AC, Gedney N, Comyn-Platt E, Hayman G, Rigby M, Poulter B, Hornibrook E (2018) Spatially Resolved Isotopic Source Signatures of Wetland Methane Emissions. Geophys Res Lett 45(8):3737–3745

Happell JD, Chanton JP, Whiting GJ, Showers WJ (1993) Stable isotopes as tracers of methane dynamics in Everglades marshes with and without active populations of methane oxidizing bacteria. J Geophys Res Atmos 98:14771–14782

Hirota M, Tang YH, Hu QW, Hirata S, Kato T, Mo WH, Cao GM, Mariko S (2004) Methane emissions from different vegetation zones in a Qinghai-Tibetan Plateau wetland. Soil Biol Biochem 36:737–748

Jackson RB, Saunois M, Bousquet P, Canadell JG, Poulter B, Stavert AR, Bergamaschi P, Niwa Y, Segers A, Tsuruta A (2020) Increasing anthropogenic methane emissions arise equally from agricultural and fossil fuel sources. Environ Res Lett 15(7):071002

Kato T, Yamada K, Tang Y, Yoshida N, Wada E (2013) Stable carbon isotopic evidence of methane consumption and production in three alpine ecosystems on the Qinghai-Tibetan Plateau. Atmos Environ 77:338–347

Keeling CD (1958) The concentration and isotopic abundances of atmospheric carbon dioxide in rural areas. Geochim Cosmochim Acta 13:322–334

Kirschke S, Bousquet P, Ciais P, Saunois M, Canadell JG, Dlugokencky EJ, Bergamaschi P, Bergmann D, Blake DR, Bruhwiler L, Cameron-Smith P, Castaldi S, Chevallier F, Feng L, Fraser A, Heimann M, Hodson EL, Houweling S, Josse B, Fraser PJ, Krummel PB, Lamarque J-F, Langenfelds RL, Le Quere C, Naik V, O'Doherty S, Palmer PI, Pison I, Plummer D, Poulter B, Prinn RG, Rigby M, Ringeval B, Santini M, Schmidt M, Shindell DT, Simpson IJ, Spahni R, Steele LP, Strode SA, Sudo K, Szopa S, van der Werf GR, Voulgarakis A, van Weele M, Weiss RF, Williams JE, Zeng G (2013) Three decades of global methane sources and sinks. Nat Geosci 6:813–823

Lowry D, Holmes CW, Rata ND, O'Brien P, Nisbet EG (2001) London methane emissions: Use of diurnal changes in concentration and $\delta^{13}C$ to identify urban sources and verify inventories. J Geophys Res Atmos 106(D7):7427–7448

Morimoto S, Fujita R, Aoki S, Goto D, Nakazawa T (2017) Long-term variations of the mole fraction and carbon isotope ratio of atmospheric methane observed at Ny-angstrom lesund, Svalbard from 1996 to 2013. Tellus Ser B-Chem Phys Meteorol 69(1):1380497

Nakagawa F, Yoshida N, Sugimoto A, Wada E, Yoshioka T, Ueda S, Vijarnsorn P (2002) Stable isotope and radiocarbon compositions of methane emitted from tropical rice paddies and swamps in Southern Thailand. Biogeochem 61:1–19

Nisbet EG, Dlugokencky EJ, Bousquet P (2014) Methane on the Rise-Again. Sci 343(493–4):95

Nisbet EG, Fisher RE, Lowry D, France JL, Zazzeri G (2020) Methane mitigation: methods to reduce emissions, on the path to the Paris Agreement. Rev Geophys 58(1):e2019RG000675

Pataki DE, Ehleringer JR, Flanagan LB, Yakir D, Bowling DR, Still CJ, Buchmann N, Kaplan JO, Berry JA (2003) The application and interetation of Keeling plots in terrestrial carbon cycle research. Global Biogeochem Cycl. https://doi.org/10.1029/2001GB001850

Peng H, Hong B, Hong Y, Zhu Y, Cai C, Yuan L, Wang Y (2015) Annual ecosystem respiration variability of alpine peatland on the eastern Qinghai-Tibet Plateau and its controlling factors.

Environ Monit Assess. https://doi.org/10.1007/s10661-015-4733-x

Peng HJ, Guo Q, Ding HW, Hong B, Zhu YX, Hong YT, Cai C, Wang Y, Yuan LG (2019) Multi-scale temporal variation in methane emission from an alpine peatland on the Eastern Qinghai-Tibetan Plateau and associated environmental controls. Agric Meteorol 276:11

Popp TJ, Chanton JP, Whiting GJ, Grant N (1999) Methane stable isotope distribution at a Carex dominated fen in north central Alberta. Global Biogeochem Cycl 13:1063–1077

Quay PD, King SL, Lansdown JM, Wilbur DO (1988) Isotopic composition of methane released from wetlands: implications for the increase in atmospheric methane. Global Biogeochem Cycl 2:385–397

Rao DK, Bhattacharya SK, Jani RA (2008) Seasonal variations of carbon isotopic composition of methane from Indian paddy fields. Global Biogeochem Cycl. https://doi.org/10.1029/2006GB002917

Rockmann T, Eyer S, van der Veen C, Popa ME, Tuzson B, Monteil G, Houweling S, Harris E, Brunner D, Fischer H, Zazzeri G, Lowry D, Nisbet EG, Brand WA, Necki JM, Emmenegger L, Mohn J (2016) In situ observations of the isotopic composition of methane at the Cabauw tall tower site. Atmos Chem Phys 16:10469–10487

Schütz H, Rennenberg H (1991) Role of plants in regulating the methane flux to the atmosphere. Trace Gas Emissions Plants. https://doi.org/10.1016/B978-0-12-639010-0.50007-8

Sherwood OA, Schwietzke S, Arling VA, Etiope G (2017) Global inventory of gas geochemistry data from fossil fuel, microbial and burning sources, version 2017. Earth Syst Sci Data 9:639–656

Song WM, Wang H, Wang GS, Chen LT, Jin ZN, Zhuang QL, He JS (2015) Methane emissions from an alpine wetland on the Tibetan Plateau: Neglected but vital contribution of the nongrowing season. J Geophys Res-Biogeosci 120:1475–1490

Sriskantharajah S, Fisher RE, Lowry D, Aalto T, Hatakka J, Aurela M, Laurila T, Lohila A, Kuitunen E, Nisbet EG (2012) Stable carbon isotope signatures of methane from a Finnish subarctic wetland. Tellus Ser B-Chem Phys Meteorol. https://doi.org/10.3402/tellusb.v64i0.18818

Stevens CM, Engelkemeir A (1988) Stable carbon isotopic composition of methane from some natural and anthropogenic sources. J Gerontol Ser A Biol Med Sci 93:725–733

Thottathil SD, Prairie YT (2021) Coupling of stable carbon isotopic signature of methane and ebullitive fluxes in northern temperate lakes. Sci Total Environ 777:146117

Ueyama M, Yazaki T, Hirano T, Futakuchi Y, Okamura M (2020) Environmental controls on methane fluxes in a cool temperate bog. Agric Meteorol 281:13

Umezawa T, Machida T, Aoki S, Nakazawa T (2012) Contributions of natural and anthropogenic sources to atmospheric methane variations over western Siberia estimated from its carbon and hydrogen isotopes. Global Biogeochem Cycl 26:15

Walter KM, Chanton JP, Chapin FS, Schuur EAG, Zimov SA (2008) Methane production and bubble emissions from arctic lakes: isotopic implications for source pathways and ages. J Geophys Res-Biogeosci 113:16

Wang M, Yang G, Gao Y, Chen H, Wu N, Peng C, Zhu Q, Zhu D, Wu J, He Y (2015) Higher recent peat C accumulation than that during the Holocene on the Zoige Plateau. Quatern Sci Rev 114:116–125

Wei D, Xu R, Tarchen T, Dai D, Wang Y, Wang Y (2015) Revisiting the role of CH4 emissions from alpine wetlands on the Tibetan Plateau: evidence from two *in-situ* measurements at 4758 and 4320m above sea level. J Geophys Res-Biogeosci 120:1741–1750

Xiang S, Guo R, Wu N, Sun S (2009) Current status and future prospects of Zoige Marsh in Eastern Qinghai-Tibet Plateau. Ecol Eng 35:553–562

Yang M, Nelson FE, Shiklomanov NI, Guo D, Wan G (2010) Permafrost degradation and its environmental effects on the Tibetan Plateau: a review of recent research. Earth Sci Rev 103:31–44

Yang G, Peng C, Chen H, Dong F, Wu N, Yang Y, Zhang Y, Zhu D, He Y, Shi S, Zeng X, Xi T, Meng Q, Zhu Q (2017) Qinghai–tibetan plateau peatland sustainable utilization under anthropogenic disturbances and climate change. Ecosyst Health Sustain. https://doi.org/10.1002/ehs2.1263

Yao L, Zhao Y, Gao S, Sun J, Li F (2011) The peatland area change in past 20 years in the Zoige Basin, eastern Tibetan Plateau. Front Earth Sci. https://doi.org/10.1007/s11707-011-0178-x

Zhang G, Zhang X, Ji Y, Ma J, Xu H, Cai Z (2011) Carbon isotopic composition, methanogenic pathway, and fraction of CH4 oxidized in a rice field flooded year-round. J Geophys Res-Biogeosci. https://doi.org/10.1007/s11707-011-0178-x

Zhang L, Xia X, Liu S, Zhang S, Li S, Wang J, Wang G, Gao H, Zhang Z, Wang Q, Wen W, Liu R, Yang Z, Stanley EH, Raymond PA (2020) Significant methane ebullition from alpine permafrost rivers on the East Qinghai-Tibet Plateau. Nat Geosci 13:349–435

Zhang G, Nan Z, Zhao L, Liang Y, Cheng G (2021) Qinghai-Tibet Plateau wetting reduces permafrost thermal responses to climate warming. Earth Planet Sci Lett 562:116858